DOI: 10.1002/cphc.200600524

Size-Dependent Structural Evolution and Chemical Reactivity of Gold Clusters

Bokwon Yoon,[b] Pekka Koskinen,[a, c] Bernd Huber,[a, c] Oleg Kostko,[c] Bernd von Issendorff,[c] Hannu Häkkinen,[d] Michael Moseler,*[a, c] and Uzi Landman*[b]

Ground-state structures and other experimentally relevant isomers of Au_{15}^- to Au_{24}^- clusters are determined through joint first-principles density functional theory and photoelectron spectroscopy measurements. Subsequent calculations of molecular O_2 adsorption to the optimal cluster structures reveal a size-dependent reactivity pattern that agrees well with earlier experiments. A detailed analysis of the underlying electronic structure shows that the chemical reactivity of the gold cluster anions can be elucidated in terms of a partial-jellium picture, where delocalized electrons occupying electronic shells move over the ionic skeleton, whose geometric structure is strongly influenced by the directional bonding associated with the highly localized "d-band" electrons.

1. Introduction

The atomic (geometric) and electronic structure of gas-phase and supported clusters (particularly gold clusters[1–13]) and the dependence of these properties, as well as their chemical and catalytic activities,[14–22] on the size of the clusters (on an atom-by-atom level), are among the foremost challenges of modern cluster science and have been the subject of growing research activities. Early studies have shown that the reactivities of small gas-phase gold clusters (Au_n in the range of up to 30 atoms) depend on the number of atoms and the charge state of the clusters, with cluster anions with an even n showing enhanced reactivity.[23,24] These observations were confirmed and extended more recently,[25,26] including observations of odd–even oscillations in the O_2 adsorption probability, which correlate with those measured for vertical detachment energies (*vDE*s).[27] It has been shown theoretically that the reactivity toward oxygen of gold cluster anions originates from their propensity to transfer electronic charge into the antibonding $2\pi^*$ orbital of molecular oxygen, thus weakening the O–O bond which becomes activated into a superoxo- or peroxo-like state; a similar charging effect occurs upon bonding of CO to charged (gas-phase or supported) gold clusters.[16]

The atomic structures of gold clusters, and their size-dependent evolution, is especially intriguing. In particular, the ionic skeleton of gold cluster anions adopts unusual geometries due to relativistically enhanced s–d hybridization;[3] the consequent directional bonding results in the preference of planar ground states for relatively large cluster sizes (at least up to Au_{12}^-),[2–4] and the occurrence of cagelike[7] and tetrahedral[5] structures for Au_{16}^- to Au_{20}^-.

Here we report on combined density functional theory (DFT) and photoelectron spectroscopy (PES) studies of Au_n^- clusters for $n = 15$ to 24, which is a size range of particular interest for understanding the nanocatalytic activity of gold clusters. The structural evolution pattern of the DFT ground states is characterized by a rich sequence of motifs: flakes→cages→tetrahedra→double-layer structures→nanocapsules (nanotubes). For certain cluster sizes, the isomers in the experimental cluster beam exhibit deviations from this sequence, indicating kinetic hindrance for formation of these ground-state structures under our experimental conditions. A detailed analysis of the Au_n^- electronic orbitals explains the enhanced reactivity of Au_{18}^- and Au_{20}^-, as well as the anomalous absence of O_2 take-up for Au_{16}^- (thus breaking the odd–even alternating pattern). These insights are based on shell-closing effects in a partial-jellium picture for the delocalized Au 6s electrons that move in the confining potential of the underlying cagelike, or tetrahedral, ionic skeleton, whose structure is determined largely by the directional bonding of the highly localized "d-band" electrons.

The Article is organized as follows: In the Methods Section we describe briefly the experimental and theoretical methods used in our study. Our results for bare gold cluster anions,

[a] *Dr. P. Koskinen, B. Huber, Dr. M. Moseler*
Fraunhofer Institute for Mechanics of Materials
Wöhlerstrasse 11, 79108 Freiburg (Germany)
Fax:(+49) 761 5142 110
E-mail: Michael.Moseler@iwm.fraunhofer.de

[b] *Dr. B. Yoon, Prof. U. Landman*
School of Physics, Georgia Institute of Technology
Atlanta, Georgia 30332-0430 (USA)
Fax: (+1) 404-894-7747
E-mail: Uzi.Landman@physics.gatech.edu

[c] *Dr. P. Koskinen, B. Huber, O. Kostko, Prof. B. v. Issendorff, Dr. M. Moseler*
Faculty of Physics, University of Freiburg
79104 Freiburg (Germany)

[d] *Prof. H. Häkkinen*
Department of Physics, NanoScience Center
University of Jyväskylä, FIN-40014 Jyväskylä (Finland)

Au_n^- $n = 14$–24, are given in Section 2.1 and those for the adsorption of oxygen to these clusters anions are given in Section 2.2. A partial-jellium scheme is described in Section 2.3. We summarize our results in Section 3.

Methods Section

The atomic and electronic structures of gold cluster anions, with and without a molecularly adsorbed oxygen dimer, were determined by solving the Kohn–Sham (KS) equations using the Born–Oppenheimer local-spin-density molecular dynamics (BO-LSD-MD) method[28] in the generalized gradient approximation (GGA).[29] The $5d^{10}6s^1$ and $2s^22p^4$ valence electrons of Au and O, respectively, were described by scalar-relativistic norm-conserving pseudopotentials.[30] The KS orbitals were expanded in a plane-wave basis with a kinetic-energy cutoff of 62 Ry. The BO-LSD-MD method does not employ a supercell, that is, periodic images of the atoms, and is thus suitable for accurate calculations for charged finite clusters.[28]

A variety of candidate structures for Au_n^- were constructed by extrapolating motifs from earlier studies on gold clusters, geometrical constructions based on smaller clusters, and via a genetic isomer search using a recently developed non-orthogonal tight-binding potential.[31] Ground-state (GS) structures and energetically lowest-lying isomers were determined by structural optimization of the clusters employing a steepest-descent-like method.

It has been reported that the DFT ground states of small gold cluster anions do not always reproduce experimental mobility data or spectroscopic information.[2,4] To identify the relevant isomers for gas-phase catalytic experiments in the size range $n = 15$ to 24, the DFT electronic density of states (DOS) was compared to high-resolution photoelectron spectra of cold (200 ± 50 K) Au_n^- clusters recorded at a photon energy of 6.42 eV. The experimental setup has been described earlier.[32,33] It is pertinent to note that our PES exhibits a characteristic uncertainty of the energy axis of less than 30 meV.

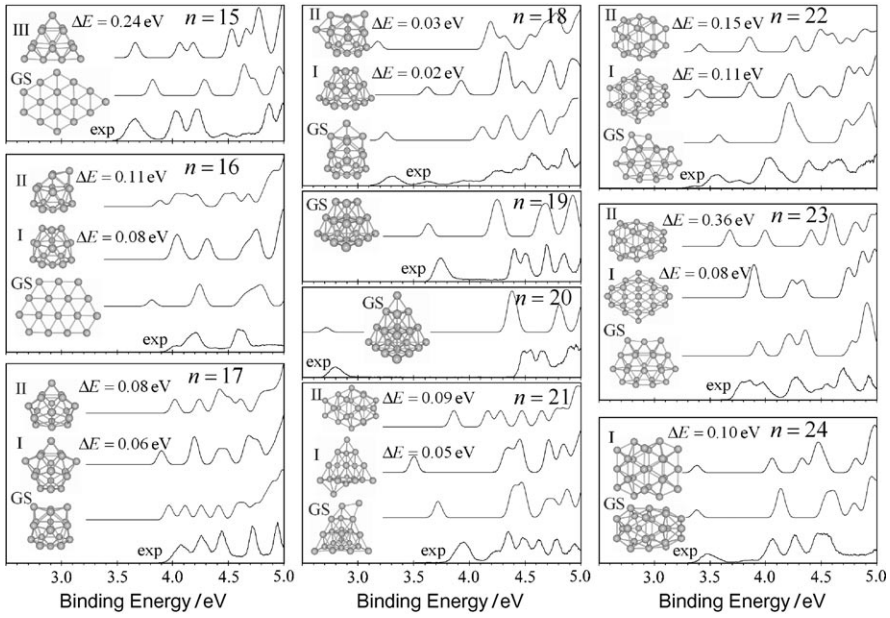

Figure 1. Structural evolution of gold cluster anions Au_{15}^- to Au_{24}^-. Shown are ground states (GS) and energetically higher-lying isomers (I, II, III, and IV). The corresponding calculated electronic densities of states are compared to experimental photoelectron spectra (curves at the bottom of each panel, marked exp). ΔE denotes the total energy difference of the isomers relative to the GS structure. Note that isomers I and II of Au_{15}^- are not displayed, since they are also planar and energetically close to the GS. The same holds for isomers II and III of Au_{21}^-, which differ from isomer I only in the adsorption site of the adatom on the Au_{20}^- tetrahedral unit.

2. Results and Discussion

2.1. Gold Cluster Anions Au_n^- ($n = 15$–24)

Figure 1 shows the important isomers of $Au^<_{15}{}^-$ to Au_{24}^- together with a comparison of the respective calculated DOS with the corresponding measured PES. Our results for the reduced size range Au_{15}^- to Au_{19}^- essentially confirm (with a few exceptions, see below) the results of a recent investigation.[7] In the following, we discuss the structural families found in our study.

Flakes

Surprisingly, and contrary to the findings in ref. [7], our ground states of the Au_{15}^- and Au_{16}^- clusters are fragments of an Au(111) plane. However, comparisons of their DOS signature with the PES data indicate that in both cases, three-dimensional (3D) isomers were measured experimentally suggesting an obvious kinetic hindrance for the formation of these flakes.

Cages

For Au_{17}^- and Au_{18}^-, cagelike structures are predicted to lie lower in energy than the energetically lowest planar isomers. Determination of the member of the cage family whose DOS fits best the experimental spectrum is a challenging task. Considering the small energies between the isomers, we conclude that the PES consists most likely of a weighted superposition of spectra corresponding to the lowest-lying isomers (see especially the small features in the PES of Au_{18}^- in the energy range 3.5–4.1 eV which are reflected in the DOS of isomer I).

Tetrahedra

For Au_{19}^-, Au_{20}^-, and Au_{21}^-, the cage-based motif is replaced by tetrahedra-based ground states. The correspondence between the respective PES traces and the DOS of the Au_{19}^- truncated tetrahedral GS and the Au_{20}^- complete tetrahedral GS supports this structural assignment (see also refs. [5,7]). On the other hand, the DOS of the cagelike isomer (IV) for Au_{21}^- yields

a superior fit to the PES data relative to the tetrahedral-based structures (GS and I–III).

Double Layers

A novel double-layer motif is found for Au_{22}^- and Au_{23}^-. The DOS/PES comparison indicates the experimental abundance of our "pitta-pocket-like" ground states, although higher-lying cagelike isomers also contribute to the spectrum.

Capsules

Au_{24}^- exhibits a remarkable ground state—a nanocapsule built by rolling an 18-atom Au(111) flake into a small cylinder with additional end-caps. This tubelike structure thus consists of stacked six-member rings, with the outer rings capped by three-atom triangles. There appears to be no relationship between this structure of Au_{24}^- and the tubelike structure suggested recently for Au_{26}^-[34] for which there is no experimental evidence. Interestingly, this theoretical construction rule is identical to the graphene-sheet rolling prescription used for carbon nanotubes. For this capsule, the calculated DOS and measured PES data are in reasonable agreement, even though the DOS of a double-layer isomer (I) provides an equally good fit to the experiments.

2.2. Oxygen Adsorption on Gold Cluster Anions

We turn next to the size-dependent evolution of the chemical reactivity of the Au_n^- clusters, gauged through examination of the energetics of molecular O_2 adsorption and its correlation with the size-dependent electronic structure of the bare cluster anions. For each cluster size, the low-energy isomer, whose DOS and, in particular, whose vertical detachment energy (*vDE*, see Figure 2), conformed with the experimental PES data, was selected for a subsequent DFT calculations pertaining to the adsorption of O_2. Figure 2 (bottom) displays the energetically optimal O_2 bonding sites on the selected Au_n^- isomers. Note, that O_2 prefers to absorb at low-coordinated gold atoms, in accord with the trend observed previously for smaller clusters.[18] The O_2 binding energies $BE(O_2)$ (filled squares in Figure 2) are below 0.4 eV, except for Au_{18}^- (0.7 eV), Au_{20}^- (0.9 eV), and Au_{22}^- (0.6 eV). This finding is in excellent agreement with the experimental $Au_nO_2^-$ mass spectra,[26] which shows no abundance of $Au_{16}O_2^-$, $Au_{24}O_2^-$, or odd-sized clusters. The trend exhibited by the binding energies is portrayed also in the variation, with cluster size, of the charging of the O_2 molecule, $\delta Q(O_2)$, and the O–O bond distance, $d(O_2)$; O_2 molecules with $d(O_2) \gtrsim 1.32$ Å are in a superoxo-like state and are considered to be chemically activated [that is, a weakened O–O bond; in the gas phase $d(O_2) = 1.26$ Å]. Furthermore, the cluster-size evolution of $BE(O_2)$ displays a systematic anticorrelation with the *vDE*s (compare top two curves in Figure 2) as well as with the excess charge $\delta Q(O_2)$ and the bond length $d(O_2)$, as has been observed previously for $Au_nO_2^-$ with $n \leq 8$.[18]

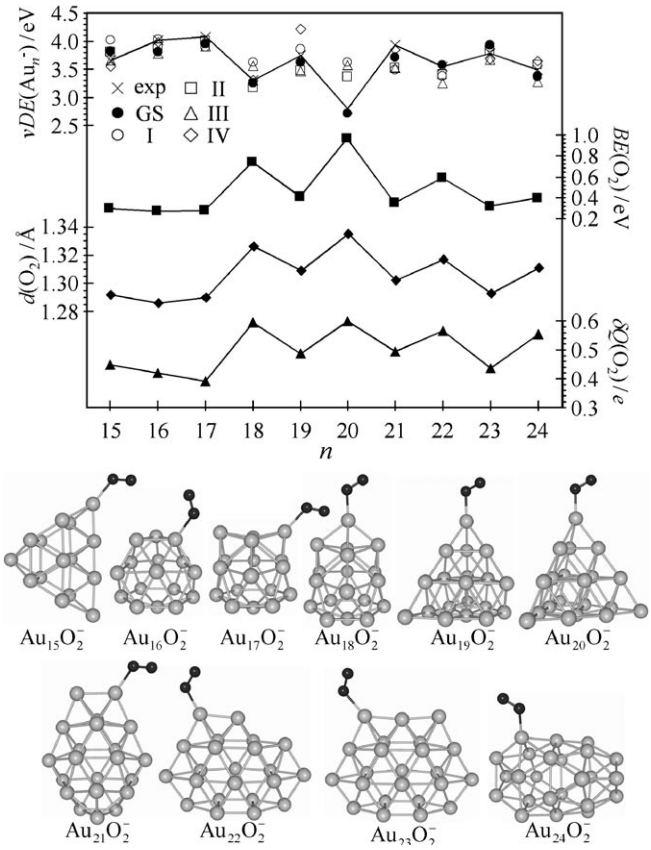

Figure 2. Top frame: Size-dependent variations of the vertical detachment energy, $vDE(Au_n^-)$, binding energy of O_2 to the optimal structures of the Au_n^- clusters, $BE(O_2)$, O–O distance of adsorbed O_2, $d(O_2)$, and excess charge on the adsorbed O_2, $\delta Q(O_2)$. In the top (*vDE*) curve the experimental results are denoted by ×, the values corresponding to the ground-state (GS) structures are displayed as ●, and the results for the higher-energy isomers (I,II,…) are denoted as indicated in the figure. Bottom: optimal adsorption geometries of O_2 (small black dots) on gold clusters (larger gray dots).

2.3. Partial-Jellium Scheme

A detailed analysis of the KS orbitals of the clusters reveal a surprisingly simple electronic-level organization that allows elucidation of the observed *vDE* and $BE(O_2)$ trends. Since it has been previously noted that closing of spin shells induces the pronounced odd–even oscillations,[27] it is instructive to focus on deviations from this behavior and on extreme *vDE* values. To illustrate the main idea, we chose to analyze the energy-level spectra of the Au_{16}^-, Au_{18}^-, and Au_{20}^- clusters. Figure 3 displays the majority-spin KS energy levels of these clusters; the minority-spin levels are not shown, since they are essentially identical to the majority spin ones. The atomic s, p, and d ($\ell = 0,1$, and 2) contribution to each KS orbital ϕ can be characterized by the weight $w\ell = \sum_{l,m} \int_0^R \left| \int Y_{\ell,m}(\Omega)\phi(\mathbf{r} + \mathbf{R}_l)d\Omega \right|^2 dr$. Here $\mathbf{R}_l$ denotes the position of the lth ion and the integration is performed in a sphere of radius R, taken to be about half of the average bond length in the cluster. The length and color of the level bars in Figure 3 quantify the contribution of atomic s and p orbitals to the KS levels, with short red bars representing the "5d-band" and long blue bars the "6s-band".

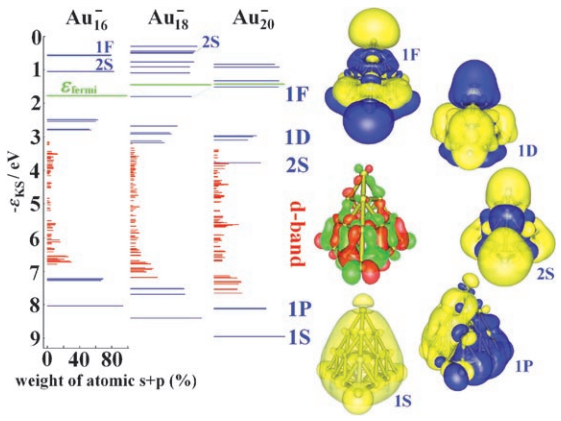

Figure 3. Majority-spin Kohn–Sham energies of the Au_{16}^- and Au_{18}^- cages and the Au_{20}^- tetrahedron. The length of the energy-level bars represents the added weight of the atomic s and p orbitals forming the KS wavefunctions. Blue bars denote high s + p weights; red bars represent states that are mostly formed by atomic d orbitals (the "d band"). The majority-spin Fermi energy is depicted in green. Isosurfaces of representative jelliumlike orbitals of Au_{20}^- are displayed on the right-hand side along with a classification into jellium-type states. Also included is an isosurface of a d state (in green and red) illustrating localization about the atomic centers that form the tetrahedral skeleton of the Au_{20}^- cluster.

A visual inspection of the isosurfaces of the "s-band" states revealed a clear jelliumlike delocalized character for all cluster sizes (see right-hand column in Figure 3 for a representative set of Au_{20}^- orbitals), allowing for a classification of these orbitals into jellium 1*S*, 1*P*, 2*S*, 1*D*, and 1*F* states.[35] In contrast, the "d-band" states exhibit a directional bonding and strong localization near the atomic nuclei.

According to this scheme, we found the following jellium configurations: $Au_{16}^- \rightarrow 1S^2 1P^6 1D^9$, $Au_{18}^- \rightarrow 1S^2 1P^6 1D^{10} 1F^1$ and $Au_{20}^- \rightarrow 1S^2 1P^6 2S^2 1D^{10} 1F^1$. The absence of the 2*S* state in Au_{18}^- is somewhat surprising since a spherical, simple metal cluster with 19 electrons exhibits a $1S^2 1P^6 1D^{10} 2S^1$ configuration.

To understand this anomaly we estimated the electron density inside a sphere with a radius of $2a_0$ centered at the center of mass of the cluster (a_0 is the Bohr radius). While for Au_{16}^- and Au_{18}^- only about 0.15 e^- is found inside this sphere, approximately 1 e^- is found for the Au_{20}^- cluster. This observation correlates well with the larger diameter of the central cavity in the Au_{16}^- and Au_{18}^- clusters compared to Au_{20}^-. We found a minimum distance between the gold atoms and the center of the cavity of 4.66 a_0 and 5.22 a_0 for Au_{16}^- and Au_{18}^-, respectively, compared to 3.57 a_0 for Au_{20}^-. In a spherical hollow jellium, the 2*S* state is destabilized since it carries too much electron density in the central region of the cluster (note that the 2*S* states of Au_{16}^- and Au_{18}^- in Figure 3 are located among the unoccupied KS states). This renders 18 electrons in a hollow jellium, a strong shell closing.

In light of the above partial-jellium-like electronic shell scheme, we discuss in the following the reactivity of the Au_n^- clusters. Within a hollow jellium model, the bare Au_{16}^- cluster lacks just a single electron for closure of a major shell (the 1*D* shell, see above). This halogen-like situation underlies the high *vDE*, of Au_{16}^- (see Figure 2) and the corresponding low O_2 binding energy (Figure 2), as well as the experimental absence of $Au_{16}O_2^-$ (see ref. [26]). On the other hand, both Au_{18}^- and Au_{20}^- behave in an alkali-like manner (the former in the hollow and the latter in the filled jellium model) with corresponding low *vDE* values and high reactivities towards O_2 (see Figure 2).

Similar partial-jellium schemes can be found for all other cluster sizes, for instance, for the strongly oblate Au_{22}^- and the tubular Au_{24}^-. However, a discussion of the reactivity is more complicated in these cases due to strong shape distortions. On the other hand, the size range of our jellium picture can be easily extended for other regularly shaped clusters; for example, the planarity in the size range $n = 4$–13 atoms is related to magic numbers of 2, 6, and 12 electrons (see, for instance, refs. [36, 37]). For these clusters, the triangular Au_6^-, with its seven delocalized electrons, has a very low *vDE*[27] (characteristic for a cluster just past a shell closing, similar to the behavior of Au_{20}^- discussed above) and the triangular Au_{10}^-, with 11 delocalized electrons, has an anomalously high *vDE*[27] (characteristic for a cluster approaching shell closure, that is, 12 e^- in 2D, in analogy with the behavior of the 3D cluster Au_{16}^-). Indeed, orbital analysis of Au_{10}^- revealed six majority spin orbitals with symmetries expected for a two-dimensional jellium.

3. Summary

We used photoelectron spectroscopy measurements and first-principles density functional calculations to explore the size-dependent structural evolution and chemical reactivity of gold cluster anions, Au_n^- ($n = 15$–24 atoms). For each cluster size, we optimized several structural isomers and found that while in some cases the calculated electronic densities of states for the ground-state structures provide the best fit to the measured PES data, in other cases the DOS corresponding to higher-lying isomers, or a superposition of the DOS of several isomers, describe the data better. This indicates that under experimental conditions, it is not always possible to anneal the clusters to their ground-state structure. The calculated ground states revealed an interesting evolution (Figure 1), from 2D flaky structures for $n = 15$ and 16 (although, most likely, due to kinetic hindrance, the 3D isomers dominate experimentally) to 3D cages for $n = 17$ and 18, tetrahedra for $n = 19$–21, double-layer (pitta-pocket-like) structures for $n = 22$ and 23, and a capsule (capped nanotube-like) for $n = 24$.

Detailed investigation of the adsorption of O_2 to the optimal structures of Au_n^- revealed preferred binding to a low-coordinated site via anchoring the molecule through one of its atoms (Figure 2). The binding energies exhibit odd–even alternation that correlates well with the O–O bond lengths and the excess charge on the adsorbed molecules, which are activated to a superoxo-like state for gold anion clusters with an even number of atoms. On the other hand, the binding energies anticorrelate (minima in one correspond to maxima in the other) with the corresponding vertical detachment energies (measured and calculated, which agree well with each other).

The reactivity pattern of the clusters, gauged through the oxygen adsorption propensity, and the size variation of the *vDE* records are elucidated with the use of a partial-jellium pic-

ture, where we have shown that delocalized electrons (originating from the least-bound atomic 6s state that move in the field of the ionic skeleton, whose bonding and structure are determined mostly by the localized and directional d-state electrons) organize into jelliumlike shells (Figure 3). The filling scheme of these shells correlates with the aforementioned systematics of the observed reactivity pattern, as well as with certain noted anomalies, such as the inertness of Au_{16}^- toward oxygen adsorption.

Acknowledgements

The work of B.Y. and U.L. was supported by the Air Force Office of Scientific Research and the US Department of Energy. P.K., B.H., O.K., B.v.I., and M.M. acknowledge funding of the Deutsche Forschungsgemeinschaft. Further funding was provided by the Academy of Finland for H.H. and P.K. Calculations were performed at the Georgia Tech Center for Computational Materials Science, at the National Energy Research Scientific Computing Center (NERSC) at Berkeley CA, and at the John von Neumann-Institute for Computing (NIC) in Jülich.

Keywords: chemical reactivity · density functional calculations · gold · photoelectron spectroscopy · structure elucidation

[1] H. Häkkinen, U. Landman, *Phys. Rev. B* **2000**, *62*, R2278.
[2] F. Furche, R. Ahlrichs, P. Weis, C. Jacob, S. Gilb, T. Bierweiler, M. M. Kappes, *J. Chem. Phys.* **2002**, *117*, 6982.
[3] H. Häkkinen, M. Moseler, U. Landman, *Phys. Rev. Lett.* **2002**, *89*, 033401.
[4] H. Häkkinen, B. Yoon, U. Landman, X. Li, H.-J. Zhai, L.-S. Wang, *J. Phys. Chem. A* **2003**, *107*, 6168.
[5] J. Li, X. Li, H.-J. Zhai, L.-S. Wang, *Science* **2003**, *299*, 864.
[6] H. Häkkinen, M. Moseler, O. Kostko, N. Morgner, M. A. Hoffmann, B. von Issendorff, *Phys. Rev. Lett.* **2004**, *93*, 093401.
[7] S. Bulusu, X. Li, L.-S. Wang, X. C. Zeng, *Proc. Natl. Acad. Sci. USA* **2006**, *103*, 8326.
[8] M. P. Johansson, *Angew. Chem.* **2004**, *116*, 2732; *Angew. Chem. Int. Ed.* **2004**, *43*, 2678.
[9] X. Gu, M. Ji, S. H. Wei, X. G. Gong, *Phys. Rev. B* **2004**, *70*, 205401.
[10] H. Gronbeck, P. Broqvist, *Phys. Rev. B* **2005**, *71*, 073408.
[11] R. M. Olson, S. Varganov, M. S. Gordon, H. Metiu, S. Chretien, P. Piecuch, K. Kowalski, S. A. Kucharski, M. Musial, *J. Am. Chem. Soc.* **2005**, *127*, 1049.
[12] Y. K. Han, *J. Chem. Phys.* **2006**, *124*, 024316.
[13] E. M. Fernandez, J. M. Soler, L. C. Balbas, *Phys. Rev. B* **2006**, *73*, 235433.
[14] M. Haruta, *Catal. Today* **1997**, *36*, 153.
[15] A. Sanchez, S. Abbet, U. Heiz, W.-D. Schneider H. Häkkinen, R. N. Barnett, U. Landman, *J. Phys. Chem. A* **1999**, *103*, 9573.
[16] B. Yoon, H. Häkkinen, U. Landman, A. S. Wörz, J.-M. Antonietti, S. Abbet, K. Judai, U. Heiz, *Science* **2005**, *307*, 403.
[17] H. Häkkinen, S. Abbet, A. Sanchez, U. Heiz, U. Landman, *Angew. Chem.* **2003**, *115*, 1335; *Angew. Chem. Int. Ed.* **2003**, *42*, 1297.
[18] B. Yoon, H. Häkkinen, U. Landman, *J. Phys. Chem. A* **2003**, *107*, 4066.
[19] G. Mills, M. S. Gordon, H. J. Metiu, *J. Chem. Phys.* **2003**, *118*, 4198.
[20] L. M. Molina, D. Hammer, *J. Catal.* **2005**, *233*, 399.
[21] N. Lopez, J. K. Norskov, *J. Am. Chem. Soc.* **2002**, *124*, 11262.
[22] U. Heiz, U. Landman, *Nanocatalysis*, Springer, Berlin, **2006**.
[23] D. M. Cox, R. Brickman, K. Creegan, A. Kaldor, *Z. Phys. D* **1991**, *19*, 353.
[24] D. M. Cox, R. Brickman, K. Creegan, A. Kaldor, *Mater. Res. Soc. Symp. Proc.* **1991**, *206*, 43.
[25] B. E. Salisbury, W. T. Wallace, R. L. Whetten, *Chem. Phys.* **2000**, *262*, 131.
[26] Y. D. Kim, M. Fischer, G. Ganteför, *Chem. Phys. Lett.* **2003**, *377*, 170.
[27] K. J. Taylor, C. L. Petiette-Hall, O. Cheshnovsky, R. E. Smalley, *J. Chem. Phys.* **1992**, *96*, 3319.
[28] R. N. Barnett, U. Landman, *Phys. Rev. B* **1993**, *48*, 2081.
[29] J. P. Perdew, K. Burke, M. Ernzerhof, *Phys. Rev. Lett.* **1996**, *77*, 3865.
[30] N. Troullier, J. L. Martins, *Phys. Rev. B* **1991**, *43*, 1993.
[31] P. Koskinen, H. Häkkinen, G. Seifert, S. Sanna, T. Fraunheim, M. Moseler, *New J. Phys.* **2006**, *8*, 9.
[32] M. Astruc Hoffmann, G. Wrigge, B. von Issendorff, *Phys. Rev. B* **2002**, *66*, 041404R.
[33] G. Wrigge, M. Astruc Hoffmann, B. von Issendorff, *Phys. Rev. A* **2002**, *65*, 063201.
[34] W. Fa, J. Dong, *J. Chem. Phys.* **2006**, *124*, 114310.
[35] W. de Heer, *Rev. Mod. Phys.* **1993**, *65*, 611.
[36] S. Reimann, M. Koskinen, H. Häkkinen, P. E. Lindelof, M. Manninen, *Phys. Rev. B* **1997**, *56*, 12147.
[37] E. Janssens, H. Tanaka, S. Neukermans, R. E. Silverans, P. Lievens, *New J. Phys.* **2003**, *5*, 46.

Received: August 24, 2006
Published online on November 28, 2006

